Spectroscopic Observations and Thermodynamic Calculations on Clathrate Hydrates of Mixed Gas Containing Methane and Ethane: Determination of Structure, Composition and Cage Occupancy

Tsutomu Uchida,*,† Satoshi Takeya,† Yasushi Kamata,† Ikuko Y. Ikeda,† Jiro Nagao,† Takao Ebinuma,† Hideo Narita,† Olga Zatsepina,‡ and Bruce A. Buffett‡

Gas Hydrate Reserch Group, Institute for Energy Utilization, AIST, 2−17−2−1 Tsukisamu-higashi, Toyohira-ku, Sapporo 062-8517, Japan, and Department Earth and Ocean Science, University of British Columbia, Vancouver, B.C. Canada V6T 1Z4

Received: April 3, 2002; In Final Form: September 20, 2002

Clathrate hydrates of methane−ethane mixed gases have two crystal structures depending on their composition. To study their compositions and cage occupancies and how their structure is determined, we synthesized hydrate samples from methane−ethane mixtures. Analysis of the samples using X-ray diffraction, Raman spectroscopy, and gas chromatography revealed their structures, compositions, and cage occupancies. Experimentally, hydrate structure II existed in samples formed when the gas equilibrated with hydrates was approximately 2% C_2H_6 (molar fraction) whereas both structures I (sI) and II (sII) coexisted for 12 to 22% C_2H_6. The structures below 2% and above 22% of C_2H_6 existed only as sI hydrates. Volume ratios of both structures were obtained from the ratio of the peak intensities of the C−C stretching peaks in the Raman spectra. In the transition zone containing both structures, the volume ratio of the sII structure gradually decreased with increasing C_2H_6 concentration. Cage occupancies of guest molecules in the hydrate cages were determined by the relative intensity ratio of Raman spectra. C_2H_6 molecules occupied only large cages in both structures, whereas CH_4 molecules occupied the remaining cages. The experiments agree with the structure and molecular distributions that were predicted by minimizing the Gibbs free energy of the sample. This model calculation provides insight into the structural transition mechanism.

Introduction

In recent years, gas hydrates have become recognized as a potentially large natural gas resource because huge amounts of natural gases are stored in crystalline hydrates in deep sea sediments and in permafrost.[1,2] Natural gas hydrates, which are stable at high pressure and low temperature, contain natural gases with 150 times more volume than the gas at the standard temperature and atmospheric pressure. Furthermore, storage of gas as a hydrate is safer than storage in the gas phase. To determine the feasibility of using gas hydrates as a natural resource, estimating gas volumes in the gas hydrate are needed. Such estimates require knowledge of the crystalline structure, the gas compositions of gas hydrates, and the cage occupancies of the guest molecules. In general, experimental and theoretical methods to obtain such knowledge are established, although the cage occupancies of gas hydrates are difficult to measure directly. Recently, spectroscopic analyses have been applied to cage occupancy measurements. We use Raman spectroscopy to determine the cage occupancy because it has advantages for estimating cage occupancies and gas compositions in hydrate structures.[3,4]

Light hydrocarbon molecules, such as methane (CH_4), ethane (C_2H_6), and propane (C_3H_8), are major components of natural gas. Most light hydrocarbons can become guest molecules. X-ray diffraction (XRD) analysis has shown that there are three crystalline structures for gas hydrates of light hydrocarbons: structure I (sI), structure II (sII), and structure H (sH).[5] CH_4 and C_2H_6 form sI hydrates, whereas larger guest molecules such as C_3H_8 form sII hydrates. However, the hydrate structure does not depend only on the guest molecule size because the relatively small molecules of nitrogen and oxygen also form sII hydrates.

Subramanian et al.[6] found evidence for the formation of sII hydrates in mixtures of CH_4 and C_2H_6 by using Raman and NMR spectroscopic techniques, which was supported by the modeling and experiments of Ballard and Sloan.[7] To better understand this system, we measured the hydrate structures and guest molecule concentrations of hydrates formed from various mixtures of CH_4 and C_2H_6. In the present study, we prepared mixed gas hydrates from an ice powder and various mixtures of CH_4 and C_2H_6. Then, we performed Raman spectroscopic analyses on those samples to obtain the guest molecule spectra, which was used to determine the host structure and guest composition in the hydrate phase. The crystal structures were also determined by XRD analysis on the same samples. Gas compositions of the free gas equilibrated with the hydrate and of gases extracted from the hydrate were also measured by gas chromatography (GC) to complement the cage occupancy from the Raman analysis. These experimental results were compared with the results of thermodynamic calculations. The model predictions were also used to infer the mechanism of the structural transition.

Experimental Procedures

We prepared the hydrate samples with an ice−gas interaction procedure. This system has the advantage that it produces

* To whom correspondence should be addressed. E-mail: t.uchida@aist.go.jp. Phone: +81-11-857-8965. Fax: +81-11-857-8989.
† Institute for Energy Utilization.
‡ University of British Columbia.

10.1021/jp025884i CCC: $22.00 © 2002 American Chemical Society
Published on Web 10/29/2002

homogeneous samples, which allows us to use the same sample in various measurements. In our 263.2 K cold room, approximately 30 g of ice particles, each with 1 to 2 mm diameter, were loaded into a pressure vessel of volume of approximately 1×10^{-3} m^3. A CH_4 and C_2H_6 gas mixture was then put into the vessel and initially pressurized to between 1 and 3 MPa. After the hydrate started forming on the surfaces of the ice particles, we sped up the hydrate formation rate by crushing the particles with a stirring rod inserted in the vessel (which creates new ice surfaces for the hydrate to form on). This crushing was done as the pressure vessel rotated at approximately 50 rpm. This process turned the sample into a fine powder (sizes less than 100 μm). During the reaction, the pressure in the vessel decreased by approximately 0.3 MPa relative to the initial pressure, which took approximately 24 h. The hydrate sample was cooled before depressurization to prevent rapid decomposition and was stored in a bottle at liquid nitrogen temperature to prevent sample decomposition during storage at atmospheric pressure.

The gas composition of the initial feed gas (determined by the C_2H_6 concentration: y^0_{C2}) and the gas concentration in equilibrium with the hydrates after the complete reaction (y_{C2}) were measured by an on-line gas chromatograph (GC; Shimazu model GC-14B). Usually y_{C2} was smaller than y^0_{C2} in the batch type reactor because of the preferential consumption of C_2H_6 for hydrate formation. However, the volume of the vapor was much larger than the ice volume, so the composition change in the vapor was small. The gas composition in the hydrate (y^H_{C2}) was, on the other hand, determined by an off-line GC (AREA model MC-200) that measured the gas that decomposed from the hydrate sample. The error of the GC measurement was estimated to be within 5%.

The experimental setup of the Raman spectroscopic measurements was similar to that used in our previous study.[4] The specimen was set below the objective lens and the scattered radiation was collected through a slit with 180° geometry at 200 μm. With a $\times$40 objective lens, the magnification of the system was approximately 10^3. The diameter of the incident laser-beam focused on the specimen was approximately 5 μm. The temperature of the specimen was maintained at approximately 150 K during measurements by controlling the flow speed of gas that vaporized from liquid nitrogen. The line shape of the neon emission lines indicated that the accuracy of the wavenumber measurement was approximately ± 1 cm^{-1}. Spectra were collected at a resolution determined by the 0.25 cm^{-1} scanning steps and at a 3 s integration per step. For each sample, we collected such spectra at more than six positions in the sample and averaged the spectra. Each Raman spectrum was then analyzed by deconvoluting the spectrum and fitting peaks to Lorentzian curves.

The crystal structures were determined using a Cu Kα X-ray diffractometer (40 kV, 250 mA; Rigaku model Rint-2000). The hydrate samples were loaded into a quartz glass capillary cell (Hilgenberg; 2.0 mm diameter, 0.01 mm thick) that was put on top of the goniometer. These measurements were done at 113.0 $\pm$ 1.0 K by blowing cold, dry nitrogen gas at atmospheric pressure around the sample. Phase transformations at such temperatures were negligible over the course of the measurements.

Thermodynamic Calculation of Mixed Gas Hydrates

Phase equilibrium calculations for a system composed of CH_4, C_2H_6, and H_2O were undertaken using a method previously developed for a single gas component[8] to support the experiments. We began the calculation by specifying all possible stable phases. Because of the low temperature of the experiments, H_2O can exist as ice, hydrate, and vapor. Also, CH_4 and C_2H_6 can exist in their vapor and hydrate phases but are excluded from the ice. Our calculations allow for the presence of both sI and sII hydrate but not sH.

The calculation of phase equilibrium can be viewed as an optimization problem. For fixed pressure and temperature conditions, the equilibrium state is defined by a global minimum in the Gibbs free energy G. We searched for the global minimum in G by adjusting the proportions of chemical components across all of the possible phases. Phases that are thermodynamically unstable (e.g., ice in the presence of high-pressure CH_4 and C_2H_6) disappear in the search for the global minimum in G. The Gibbs free energy is an extensive thermodynamic property, so it can be summed over the chemical potentials of each phase

$$G = \sum_{i,j} n_i^j \mu_i^j \tag{1}$$

where μ_i^j are the chemical potentials (e.g., free energies per mole) and n_i^j are the corresponding numbers of moles of the different compositions i in the various phases j. The chemical potential for the vapor mixture μ_i^V is expressed in terms of fugacity f_i^V as

$$\mu_i^V = \mu_i^0 + RT \ln(f_i^V/f_i^0) \tag{2}$$

where R is the gas constant, and μ_i^0 and f_i^0 are the chemical potential and fugacity of component i in its reference state. We use the pure vapor phases at the same P and T conditions for the reference states of CH_4, C_2H_6, and pure ice for H_2O. Fugacity f_i^V is related to the mole fraction x_i^V and the total pressure P by

$$f_i^V = \phi_i^V x_i^V P \tag{3}$$

where ϕ_i^V is the fugacity coefficient. We used the Trebble and Bishnoi equation of state[9] to calculate ϕ_i^V.

The standard thermodynamic model for the hydrate phase was developed by van der Waals and Platteeuw.[10] The chemical potential of water in this model is defined by

$$\mu_w^H = \mu_w^0 + \Delta\mu_w^\beta - \Delta\mu_w^H \tag{4}$$

where μ_w^0 is the reference state. Corrections $\Delta\mu_w^\beta$ and $\Delta\mu_w^H$ represent two distinct contributions to μ_w^H: the difference in the chemical potential of water between ice and an empty hydrate lattice and the change in the chemical potential of water affected by the enclathrated guest molecules, respectively. The former correction term is given by Holder et al.[11] The latter term is the function of the cage occupancies, which is given by

$$\Delta\mu_w^H = -RT \sum_m \nu_m \ln(1 - \sum_i \theta_{mi}) \tag{5}$$

where ν_m is the number of cages of type m per water molecule in the lattice and θ_{mi} is the fraction of type m cages occupied by guest component i. The occupancy θ_{mi} depends primarily on the fugacity f_i^V of the guest component i according to

$$\theta_{mi} = C_{mi} f_i^V/(1 + \sum_j C_{ml} f_l^V) \tag{6}$$

where C_{ml} are known as Langmuir constants. The chemical potentials of CH_4 and C_2H_6 in the hydrate structure are implicitly

established by the occupancy θ_{mi} by using the van der Waals and Platteeuw model.[10] We calculated the Langmuir constants in (6) using the spherical Kihara potential for guest−host interactions. The Kihara parameters for CH_4 and C_2H_6 are taken from Ballard and Sloan.[7] The determination of the occupancy ensures that these chemical potentials are equal to the chemical potentials of CH_4 and C_2H_6 in the surrounding vapor phase. Thus, the chemical potentials of CH_4 and C_2H_6 in the hydrate phase are given by their values in the coexisting vapor phase.

The resulting estimate of G is a nonlinear function of P, T and composition. H_2O is present in the vapor, ice, sI, and sII hydrate phases. CH_4 and C_2H_6 are included in the vapor, sI, and sII hydrate phases. When P and T are fixed, G solely depends on the numbers of moles n_i^j of different components i in the various phases j. Therefore, the problem has 10 variables: the number of moles of H_2O in vapor, ice, and the two hydrate structures, the number of moles of CH_4 in vapor and the two hydrate structures, and the number of moles of C_2H_6 in vapor and two hydrate structures.

We started the calculations with a fixed number of moles of H_2O, CH_4, and C_2H_6, which were distributed randomly over the possible phases. Conservation of H_2O, CH_4, and C_2H_6 reduces the number of independent variables from 10 to 7. Additional constraints are imposed by the model of van der Waals and Platteeuw because the occupancies of CH_4 and C_2H_6 in sI and sII hydrate are fixed by the composition of the vapor phase that coexists with the hydrate phases. These four additional constraints reduce the total number of independent variables to three. We chose to include as independent variables the number of moles of H_2O in ice and the number of moles of H_2O in sI and sII hydrates. All other variables were calculated from these three independent variables using the constraints mentioned above. The independent variables were iteratively adjusted while searching for a minimum in G.

Phase equilibrium was defined by the values of the three independent variables that minimized G. This optimization problem was solved using a simulated annealing algorithm due to Ingber.[12] The independent variables were randomly perturbed to search for the global minimum in G at fixed P and T conditions. Once the equilibrium is reached, the chemical potential of the separate components are checked to ensure equality across the coexisting phase; otherwise an adjustment of the phase proportions would lower G. This distinguishes our approach from other phase equilibrium calculations that make explicit use of the equality of chemical potentials (e.g., Englezos and Bishnoi[13]) because we do not need to know in advance which phases are stable. An alternative strategy for minimizing G was devised by Gupta et al.[14] Their study uses the condition that G is stationary with respect to the variables n_i^j to derive a set of nonlinear algebraic equations, which are solved by using a Newton−Raphson procedure. This approach should yield results that are identical to ours, although the Newton−Raphson procedure is more likely to become trapped in a local minimum and never reach the global minimum.

Results and Discussions

(a) Estimations of Hydrate Structures and Their Volume Fractions. Raman spectra in the C−C (950−1050 cm^{-1}) and C−H (2800−3000 cm^{-1}) stretching-vibration mode regions and XRD patterns were used to determine hydrate structure; in general, they gave consistent results. The C−C stretching mode spectrum was a good indicator of the type of structure formed from the CH_4−C_2H_6 system, and it provided estimates of the volume concentration of sII in samples that had both sI and sII.

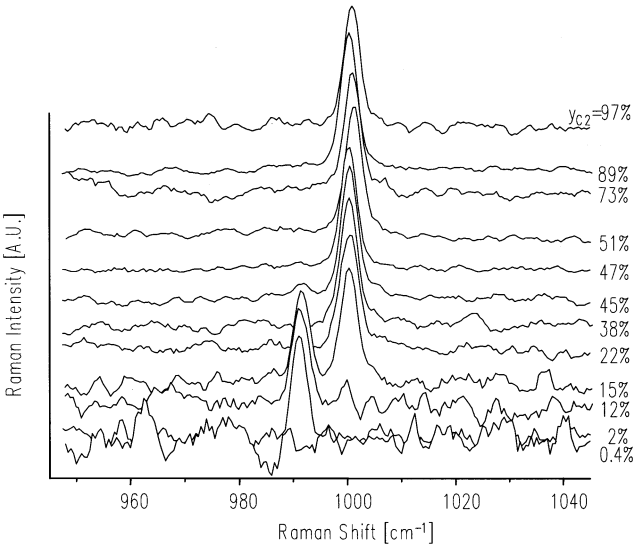

Figure 1. Raman spectra in the C−C stretching mode region at approximately 150 K. The peaks for sI and sII hydrates are at 1001.6 and 991.4 cm^{-1}, respectively. The labeled compositions of C_2H_6 (y_{C2}) in the gas were measured by GC after the hydrates formed at 263 K.

Two peaks exist in the ν_3 C−C symmetric stretching-vibration mode of C_2H_6 molecules in Figure 1: one is at approximately 1001.6 cm^{-1} and another is at 991.4 cm^{-1}. Previous measurements at about 274.2 K[6,15] found that the Raman peak for C_2H_6 trapped in the large cage of sI is at approximately 1000.9 cm^{-1} and that for C_2H_6 in the large cage of sII is at about 992.9 cm^{-1}. Hence, we assigned the 1001.6 cm^{-1} peak to C_2H_6 trapped in the large cage of sI ($5^{12}6^2$ = 12 pentagons, 2 hexagons) and the 991.4 cm^{-1} peak to C_2H_6 in the large cage of sII ($5^{12}6^4$). The difference between these values and the previous measurements is probably because the temperature is more than 100 K lower in our study. The 991.4 cm^{-1} peak was observed in the sample between y_{C2} = 2 and 22%. Therefore, we conclude that the sII hydrates formed when the final gases contained C_2H_6 between 2 and 22%, whereas sI hydrates formed in all samples except for that at y_{C2} = 2%, which formed only sII.

Two peaks existed simultaneously at y_{C2} ranging from 12 to 22%. These peaks indicate that both hydrate structures existed within the area of approximately 5 μm in diameter. This result indicates that the C−C stretching mode spectrum clearly distinguished the hydrate structures even when both structures coexisted in the same sample.

To verify this crystal structure interpretation, we measured the same samples by XRD. (Details of the XRD results are published elsewhere.[16]) The diffraction patterns clearly show which hydrate structures existed in the sample, and the structures agree with the Raman data. Hence, the Raman C−C stretching mode accurately predicted the hydrate structures in this system. The diffraction patterns also showed that ice remained in the sample.

The peaks in Figure 1 are assigned to the single ν_3 mode of C_2H_6; therefore, their relative intensities should depend linearly on the number of C_2H_6 molecules in each structure. Hence, we estimated the volume concentration of sII hydrate from the relative intensity of C−C stretching spectra of C_2H_6. The intensity of the lower wavenumber peak for sII hydrate (A_{C2}^{II}) and that of the higher peak for sI hydrate (A_{C2}^{I}) were analyzed by deconvoluting the spectrum, fitting the peak to a Lorentzian curve, and measuring the integrated peak area. Because C_2H_6 molecules were included only in the large cage and each cage was fully occupied by guest molecules (these are shown in the

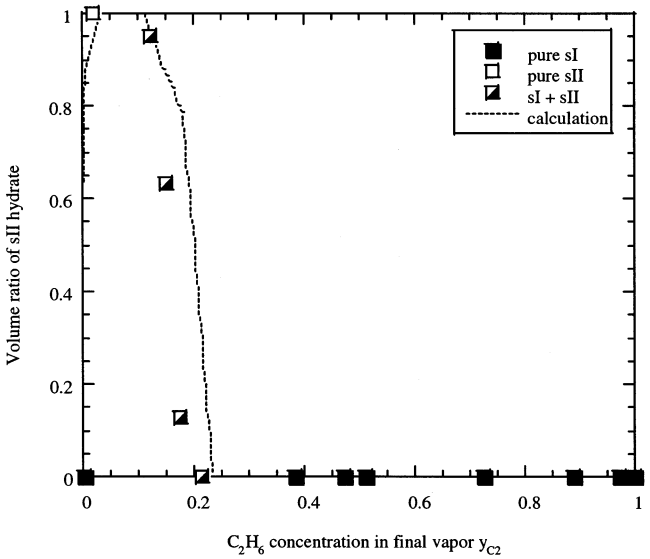

Figure 2. Volume fraction of sII hydrate as determined from the relative intensity ratio of C−C stretching spectra. The remaining concentration is a measure of the concentration of sI hydrate in the same sample. The dotted line was calculated from a thermodynamic model under the conditions of $P = 1.5$ MPa and $T = 258$ K. Solid squares are sI hydrate, open squares are sII hydrate, and their mixtures are shown by the half-solid squares. All of the structures were determined from Figure 1.

later discussion for Figure 4), we used the relative intensity ratio of C−C stretching spectra to estimate the number density ratio of C_2H_6 molecules with the collection of the difference of the large-cage number density for each structure. The number density of large cages in sI hydrate is approximately 2.1 times more than that in sII, so the volume concentration of sII hydrate was calculated from $A_{C2}{}^{II}/(A_{C2}{}^{II} + A_{C2}{}^{I}/2.1)$. The results of this estimate of volume ratio are plotted in Figure 2; when y_{C2} becomes approximately 2%, the hydrate was completely sII. When y_{C2} exceeds 12%, both sI and sII formed, and the increase of y_{C2} raises the volume ratio of sI hydrates. Finally, the hydrate is completely sI when y_{C2} exceeds 22%. Therefore, sII structure of $CH_4-C_2H_6$ hydrates formed only at small concentrations of C_2H_6 ($2\% < y_{C2} < 22\%$), and the volume ratio of sII hydrate was sensitive to y_{C2}.

The dotted line shows the prediction from the thermodynamic model. It coincides well with the experimental results. Some disagreement between theory and experiment occurred in the sI−sII transition zone, but this might have resulted from the formation process of the hydrate. For example, the C_2H_6 concentration in the vapor decreased during hydrate formation because our reaction vessel was the batch-type reactor. If the feed gas had a composition that forms both sI and sII structures, then the resulting sample could include both structures. Furthermore, the thermodynamic calculation assumed that all H_2O molecules converted from ice to hydrate, but XRD measurements showed that some H_2O molecules remained as ice.[16] This is not consistent with the assumption of the model. If this remaining ice reacted completely, the vapor would change to a slightly CH_4-richer composition. Such unreacted H_2O molecules might reduce the sII concentration below those predicted by the model.

The Raman spectra of the C−H stretching vibration region are shown in Figure 3. The figure shows two peaks for CH_4 molecules (at approximately 2902 and 2912 cm^{-1}) and three or four C_2H_6 peaks (at approximately 2887, 2923, 2943, and 2966 cm^{-1} for the sI samples and 3 cm^{-1} lower in each peak for sII). The two CH_4 peaks are assigned to ν_1 symmetrical C−H

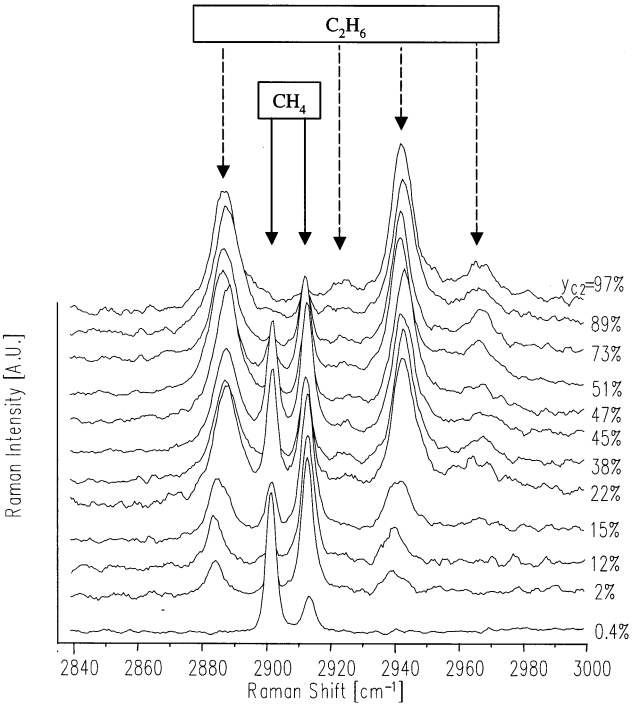

Figure 3. Raman spectra in the C−H stretching mode region at approximately 150 K. Double peaks from CH_4 molecules are at approximately 2902 and 2912 cm^{-1}. Other peaks are due to C_2H_6 molecules. The labeled concentrations of C_2H_6 (y_{C2}) were measured by GC in the gas after the hydrates formed.

stretching vibrations; one is assigned to the large cage and one to the small cage.[3,4] These are approximately 3 cm^{-1} lower in wavenumber than previous results.[3,4] This shift could be attributed to the lower temperature used in our experiments. Except in the smallest C_2H_6 concentration sample, the intensity of the lower wavenumber peak (A^L_{C1}) is smaller than that at the higher wavenumber (A^S_{C1}).[4] This indicates that CH_4 molecules mainly occupy the small cages, and they compete with C_2H_6 to occupy the large cages. Furthermore, the C−H stretching peaks for CH_4 had nearly the same positions in the different structures. (For example, see the spectrum of y_{C2}=15%, which included both structures.) This is different from the results observed on the C−C stretching spectra for the C_2H_6 molecules and indicates that the C−H stretching peaks for CH_4 cannot be used to determine the structure.

The C−H stretching spectra of CH_4 molecules indicate the number density of molecules in each cage type. The dependence of A^L_{C1}/A^S_{C1} (the relative intensity ratio of both peaks) on gas composition in the hydrate is shown in Figure 4. (The abscissa is the measured composition in the hydrate instead of that in the vapor as in Figure 2.) The dashed line is the predicted intensity ratio for the full cage occupancy of sI, whereas the dotted line is that for sII. This figure shows that the measured A^L_{C1}/A^S_{C1} rapidly decreases from approximately 3 in pure CH_4 hydrate to about 0.3 for y^H_{C2} of approximately 20% in sII hydrate. With further increase in y^H_{C2}, the measured A^L_{C1}/A^S_{C1} follows the sII hydrate line (dotted) to nearly 0 at $y^H_{C2} \sim 35\%$, at which point most large cages in the sII hydrate are occupied by only C_2H_6 molecules. Then, this ratio increases gradually up to the dashed line of the theoretical sI hydrate curve (dashed) at y^H_{C2} near 55%, which corresponds to sI + sII hydrates. At higher C_2H_6 concentrations, the ratio decreases to zero along the sI hydrate line. Thus, most data agreed with the prediction assuming the structure and the full cage occupancy. The

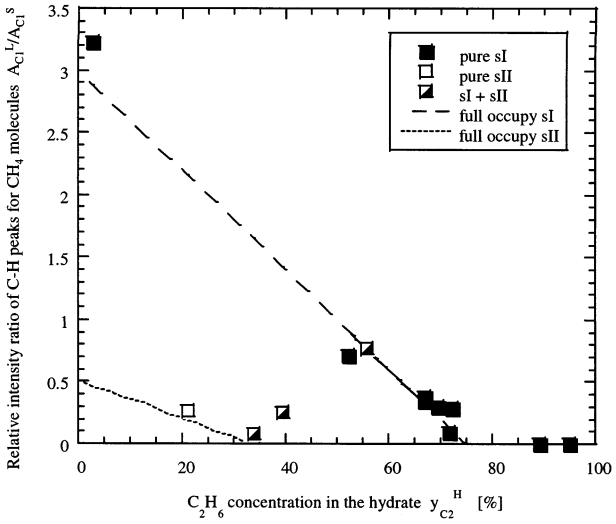

Figure 4. Relative intensity ratio A^{L}_{C1}/A^{S}_{C1} of the C−H stretching mode of CH_4 molecules in the hydrate cages. The dashed line denotes the predicted intensity ratio for full cage occupancy in sI, whereas the dotted line is that for sII. The data points in this figure were obtained on the same samples as were used for the data in Figure 2.

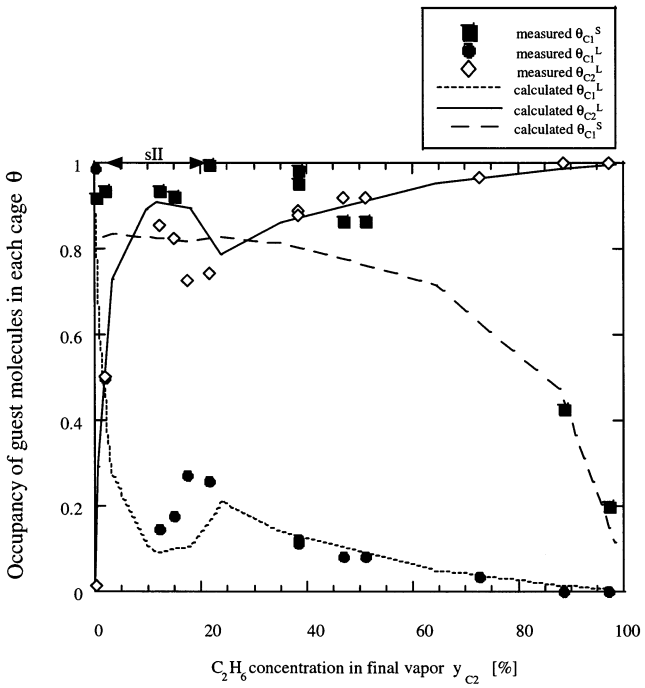

Figure 5. Occupancies of CH_4 and C_2H_6 molecules in large and small cages for various gas compositions as inferred from the Raman data. Thermodynamic model calculations (lines) were performed at $P = 1.5$ MPa and $T = 258$ K. The arrow on the top horizontal axis at the upper left indicates the range that sII hydrate occurred as determined from Figure 2.

agreement between experimental and estimated intensity ratios indicates that guest molecules almost fully occupied the hydrate cages.

The peak assignments for C_2H_6 molecule spectra assume that the strong peaks at approximately 2890 and 2940 cm^{-1} are the doublet resulting from resonance between the ν_1 symmetric C−H stretching and an overtone mode of one of the CH_3 deformation vibrations ($2\nu_{11}$).[6] These peaks are shifted by approximately 3 cm^{-1} in different structures, which agrees qualitatively with previous reports.[6,15] However, the observed C−H spectra were single peaks in the samples coexisting both structures (for example, in the sample for $y_{C2} = 15\%$, the volume of sI hydrate nearly equaled that of sII hydrate: see Figure 3). This is not because the guest molecules were included in the single type of cage but because the difference of the peak positions was too small to be distinguished.

(b) Estimations of Cage Occupancies and the Structural Transition Mechanisms. In Figure 4, we showed the calculated peak intensity ratio A^{L}_{C1}/A^{S}_{C1} of the C−H stretching mode of CH_4 molecules with full occupancy of guest molecules in each cage. The good agreement of this calculation with experimental results suggests that nearly all of the cages are occupied for the samples used in the present study. We now describe quantitative estimates of the occupancies.

Raman spectroscopy at pressures above 100 MPa showed that C_2H_6 occupies the small cage.[17,18] The latter study showed that the small peaks for the C−C stretching mode of the C_2H_6 molecules in the small cages of both hydrate structures appear at approximately 1020 cm^{-1} but only at pressures above 100 MPa. Our experiments were done at pressures far below 100 MPa, and we could not find a peak near 1020 cm^{-1} for the C_2H_6 molecules in the small cages. We therefore assumed that the occupancy of C_2H_6 molecules in small cages θ^{S}_{C2} is zero in all samples. Hence, we estimated the cage occupancies of each guest molecule in different cages with the following assumptions. (1) The concentration of CH_4 molecules in each cage depends linearly on the relative intensity ratio, A^{L}_{C1}/A^{S}_{C1}, which is the ratio of CH_4 in the large cage to that in the small cage. (2) The concentration of sII can be estimated from Figure 2. (3) C_2H_6 molecules only occupy the large cages. (4) The ratio between CH_4 and C_2H_6 in hydrates obtained from Raman measurements agrees with the composition in the hydrate phase measured by GC.

The estimated cage occupancies of guest molecules varied with the vapor compositions (Figure 5). C_2H_6 occupancy of the large cage (θ^{L}_{C2}: open diamonds) increases with the increase of C_2H_6 concentration in the vapor, especially at lower C_2H_6 concentrations. θ^{L}_{C2} reaches approximately 0.8 at $y_{C2} = 15\%$. Then, after a slight decrease, θ^{L}_{C2} increases gradually with increasing y_{C2}. The variation of occupancies of CH_4 molecules in large cages θ^{L}_{C1} (solid circles) was inverse to that from C_2H_6. On the other hand, the cage occupancy of CH_4 in the small cage (θ^{S}_{C1}: solid squares) remains constant at more than 90% until y_{C2} reaches approximately 50%. Because C_2H_6 molecules do not occupy any small cages, the variation of θ^{S}_{C1} is independent of C_2H_6 occupancy. θ^{S}_{C1} starts to decrease near $y_{C2} = 50\%$ and reaches zero at $y_{C2} = 100\%$, which is mainly because the supply of CH_4 becomes too low to fill the available cages.

Comparison of these results with the thermodynamic calculations in Figure 5 shows that the measured cage occupancies agreed qualitatively with the calculation. This result indicates that thermodynamics is useful for predicting the qualitative properties of this system. However, thermodynamics predicted θ^{S}_{C1} to be lower than measurements at low y_{C2}. The discrepancy observed at the transition zone between sI and sII might be caused by the remaining ice in the sample that did not convert to hydrate.

On the basis of our thermodynamic calculations, we briefly discuss the mechanisms of the structure change in this two-phase, multicomponent system. Incorporating C_2H_6 into the hydrate phases improves the stability of both sI and sII because the size of C_2H_6 contributes more to the stability of the large cages than CH_4. We find that the Langmuir constant for C_2H_6 in the large cage is greater in sII than it is for sI. For a

representative pressure (1.5 MPa) and temperature (258 K), the Langmuir constants for C_2H_6 in the large cages are 1271 MPa^{-1} in sII and 393 MPa^{-1} in sI. This means that C_2H_6 preferentially occupies the large cage of sII over that of sI for the same fugacity of C_2H_6 in the vapor phase and tends to enhance the stability of sII. However, sI has more large cages than sII for a given volume, and this tends to enhance the stability of sI because there is greater opportunity to incorporate C_2H_6 into sI. The competition between these two effects appears to explain the structural transition. When the bulk gas is C_2H_6 rich, a substantial fraction of the large cages of both sI and sII are filled with C_2H_6. Even though a greater fraction of the large cages in sII are filled (because of its higher Langmuir constant), sI can still contain more C_2H_6 because sI has more large cages in the same volume. Therefore, sI is the stable structure at high concentrations of C_2H_6. At low concentrations of C_2H_6, the preferential occupation of C_2H_6 in the large cages of sII favors the stability of sII. In contrast, no structural transition is predicted in mixed gas hydrates containing methane and carbon dioxide (CO_2). In this case, the Langmuir constants for CO_2 in the large cages are 34 MPa^{-1} in sII and 94 MPa^{-1} in sI at $P = 1.5$ MPa and $T = 258$ K, where the Kihara parameters used for the calculation in eq 6 are from Sloan.[5] This means that CO_2 preferentially occupies the large cage of sI, so that no competition between sI and sII exist in this case. This agrees with the experimental results.[16]

Conclusions

Methane−ethane hydrates were formed from ice particles and various gas mixtures of methane and ethane. These samples were measured by Raman spectroscopy, XRD, and GC to estimate their structures, compositions, and cage occupancies. To better understand the results and to reveal the structural transition mechanisms, the Gibbs free energy was calculated and minimized to compare predicted cage occupancies to experiment.

Each structure had different peak positions in their Raman spectra of their guest molecules. C−C stretching spectra were more sensitive to the structure type than the C−H stretching spectra. The Raman spectra indicated that structure I existed for pure CH_4 hydrate and also in the samples formed from gas including more than or equal to 12% of C_2H_6. In contrast, structure II hydrate formed only from gases of between 2 and 22% in C_2H_6 concentration. We found that both structures I and II coexisted when the vapor coexisting with the hydrates had about 12 to 22% C_2H_6. These structure determinations with the Raman spectra were confirmed by XRD analysis on the same samples. The intensity ratio of the C−C stretching spectra indicated the volume ratio of both structures in the sample. The structure change at the lower C_2H_6 concentration occurred over a narrow range of concentrations, whereas that at the higher-concentration boundary was gradual because of the mixing of both structures. The thermodynamic calculation supported the simultaneous stability of both structures in the same system.

Guest molecule distributions in each cage were determined using the Raman spectra and data from the GC measurements. C_2H_6 molecules only occupied the large cages in each structure, whereas CH_4 molecules tended to fill up the remaining large and small cages. Therefore, the gas molecule fractionation in the large cages was sensitive to the composition of the vapor phase. These experimental results agreed with the predictions from minimizing the Gibbs free energy of the system. The theoretical prediction indicated that the structural transition with the gas composition change was attributed to the interaction between two competing effects: the preferential enclathration of the C_2H_6 molecules in the large cage of structure II (because of its larger Langmuir constant under the same fugacities) and the higher concentration of large cages in structure I than that in structure II. This mechanism can also explain the absence of such a structural transition in other mixed-gases, such as methane and carbon dioxide.

Results obtained in the present study provided fundamental information for estimating total gas in mixed-gas hydrates and demonstrated the validity of spectroscopic analyses for determining physical properties of gas hydrate systems.

Acknowledgment. A part of this work was supported financially by the NEDO grant entitled "Studies on Energy Translation Technology using Clathrate Compounds" (00B60016d) and by the international joint project entitled "Research and Development on Natural Gas System utilizing Gas Hydrate Technology" collaborated with the Institute of Applied Energy. We greatly acknowledge Professor E. D. Sloan, Jr., Professor H. Lee, Mr. Y. Seo, and Mr. M. Kida for their fruitful discussions. We also thank Mr. Y. Nishikawa and Ms. M. Akaike for their support of the experiments and for preparing the manuscript.

Note Added after ASAP Posting. This article was released ASAP on 10/29/2002 with an error in eq 1. The correct version was posted on 11/05/2002.

References and Notes

(1) Paull, C. K.; Matsumoto, R.; Wallace, P. J.; et al. *Proc. ODP (Ocean Drilling Program)*, Initial Repts. *164*; College Station, TX, 1996; p 277.
(2) Dallimore, S. R.; Collett, T. S. Scientific Results from JAPEX/JNOC/GSC Mallik 2L-38 Gas Hydrate Research Well. *GSC Bulletin*; Dallimore, S. R., Uchida, T., Collett, T. S., Eds.; Mackenzie Delta: Northwest Territories, Canada, 1999; Vol. 544, p 31.
(3) Sum, A. K.; Burruss, R. C.; Sloan, E. D., Jr. *J. Phys. Chem. B* **1997**, *101*, 7371.
(4) Uchida, T.; Hirano, T.; Ebinuma, T.; Narita, H.; Gohara, K.; Mae, S.; Matsumoto, R. *AIChE J.* **1999**, *45*, 2641.
(5) Sloan, E. D., Jr. *Clathrate hydrates of natural gases*, 2nd ed.; Marcel Dekker: New York, 1998.
(6) Subramanian, S.; Kini, R. A.; Dec, S. F.; Sloan, E. D., Jr. *Chem. Eng. Sci.* **2000**, *55*, 1981.
(7) Ballard, A. L.; Sloan, E. D., Jr. *Chem. Eng. Sci.* **2000**, *55*, 5773.
(8) Zatsepina, O.; Buffett, B. *Geophys. Res. Lett.* **1997**, *24*, 1567.
(9) Trebble, M. A.; Bishnoi, P. R. *Fluid Phase Equilib.* **1988**, *40*, 1.
(10) van der Waals, J. H.; Platteeuw, J. C. *Adv. Chem. Phys.* **1959**, *2*, 1.
(11) Holder, G. D.; Corbin, G.; Papadopoulos, K. D. *Ind. Eng. Chem. Fundam.* **1980**, *19*, 282.
(12) Ingber, A. L. J. *Math. Comput. Modell.* **1989**, *12*, 967.
(13) Englezos, P.; Bishnoi, P. R. *AIChE J.* **1988**, *34*, 1718.
(14) Gupta, A. K.; Bishnoi, P. R.; Kalogerakis, N. *Fluid Phase Equilib.* **1991**, *63*, 65.
(15) Subramanian, S.; Ballard, A. L.; Kini, R. A.; Dec, S. F.; Sloan, E. D., Jr. *Chem. Eng. Sci.* **2000**, *55*, 5763.
(16) Takeya, S.; Kamata, Y.; Uchida, T.; Nagao, J.; Oyama, H.; Shimada, W.; Ebinuma, T.; Narita, H. *Proc. of 4th Int. Conf. On Gas Hydrates* **2002**, 586; Yokohama, May 19−23.
(17) Morita, K.; Nakano, S.; Ohgaki, K. *Fluid Phase Equilib.* **2000**, *169*, 167.
(18) Subramanian, S.; Sloan, E. D., Jr. *J. Phys. Chem. B* **2002**, *106*, 4348.